PTEP

Prog. Theor. Exp. Phys. **2024** 091D01 (13 pages)
DOI: 10.1093/ptep/ptae133

Missing-Mass Measurement of the $^{12}C(K^-, K^+)$ Reaction at 1.8 GeV/c with the Superconducting Kaon Spectrometer

Yudai Ichikawa [1,2,*], Jung Keun Ahn[3], Yuya Akazawa[4], Kanae Aoki[4], Elena Botta[5,6], Hiroyuki Ekawa[7], Petr Evtoukhovitch[8], Alessandro Feliciello[5], Manami Fujita[2], Toshiyuki Gogami[9], Shoichi Hasegawa[2], Tomoyuki Hasegawa[10], Shuhei Hayakawa[1], Tomonori Hayakawa[11], Ryotaro Honda[4], Kenji Hosomi[2], Ken'ichi Imai[2], Wooseung Jung[3], Shunsuke Kanatsuki[9], Shin Hyung Kim[12], Shinji Kinbara[13], Kazuya Kobayashi[11], Jaeyong Lee[14], Simonetta Marcello[5,6], Koji Miwa[1], Taejin Moon[14], Tomofumi Nagae[9], Yoshiyuki Nakada[11], Manami Nakagawa[7], Takuya Nanamura[2], Megumi Naruki[9], Atsushi Sakaguchi[11], Hiroyuki Sako[2], Yuki Sasaki[1], Susumu Sato[2], Kotaro Shirotori[15], Hitoshi Sugimura[16], Toshiyuki Takahashi[3], Hirokazu Tamura[1,2], Kiyoshi Tanida[2], Zviadi Tsamalaidze[8], Mifuyu Ukai[4], and Takeshi O. Yamamoto[2]

[1] *Department of Physics, Tohoku University, Sendai 980-8578, Japan*
[2] *Advanced Science Research Center, Japan Atomic Energy Agency, Tokai, Ibaraki 319-1195, Japan*
[3] *Department of Physics, Korea University, Seoul 02841, Republic of Korea*
[4] *Institute of Particle and Nuclear Studies (IPNS), High Energy Accelerator Research Organization (KEK), Tsukuba 305-0801, Japan*
[5] *INFN, Istituto Nazionale di Fisica Nucleare, Sez. di Torino, I-10125 Torino, Italy*
[6] *Dipartimento di Fisica, Università di Torino, I-10125 Torino, Italy*
[7] *High Energy Nuclear Physics Laboratory, RIKEN , Wako 351-0198, Japan*
[8] *Joint Institute for Nuclear Research, Dubna, Moscow Region 141980, Russia*
[9] *Department of Physics, Kyoto University, Kyoto 606-8502, Japan*
[10] *Allied Health Sciences, Kitasato University, Sagamihara 252-0373, Japan*
[11] *Department of Physics, Osaka University, Osaka 560-0043, Japan*
[12] *Department of Physics, Kyungpook National University, Daegu 41566, Republic of Korea*
[13] *Physics Department, Gifu University, 1-1 Yanagido, Gifu 501-1193, Japan*
[14] *Department of Physics and Astronomy, Seoul National University, Seoul 08826, Republic of Korea*
[15] *Research Center for Nuclear Physics (RCNP), Osaka University, Osaka 567-0047, Japan*
[16] *Accelerator Laboratory, High Energy Accelerator Research Organization (KEK), Tsukuba 305-0801, Japan*
*Email: yudai.ichikawa.d3@tohoku.ac.jp

Received May 8, 2024; Revised August 19, 2024; Accepted August 26, 2024; Published August 27, 2024

We performed a measurement of the inclusive missing-mass spectrum of the $^{12}C(K^-, K^+)$ reaction at an incident beam momentum of 1.8 GeV/c. This measurement was carried out by using the Superconducting Kaon Spectrometer (SKS) and the K1.8 beamline spectrometer at the Hadron Experimental Facility in J-PARC. From the missing-mass of the $^{12}C(K^-, K^+)$ reaction, the binding energy of a Ξ^- hyperon in a core ^{11}B nucleus, B_{Ξ^-}, can be calculated. Our experimental setup yielded a good energy resolution of 8.2 MeV (full width at half maximum), which allowed us to observe significant enhancements in the proximity of the $^{12}_{\Xi}Be$ production threshold region. In order to extract information from the missing-mass spectrum, we employed several fitting parameters assumptions. A good agreement with the spectrum shape was obtained by adding two Gaussian functions, with the constant experimental resolution for the Ξ-hypernuclear states, to the background distri-

bution. The peak positions were obtained to be $B_{\Xi^-} = 8.9 \pm 1.4$ (stat.) $^{+3.8}_{-3.1}$ (syst.) MeV and $B_{\Xi^-} = -2.4 \pm 1.3$ (stat.) $^{+2.8}_{-1.2}$ (syst.) MeV. Another model assumption, one Breit–Wigner function with $B_{\Xi^-} = -2.7 \pm 2.2$ (stat.) $^{+0.5}_{-0.7}$ (syst.) MeV and $\Gamma = 4.1 \pm 2.1$ (stat.) $^{+1.2}_{-0.7}$ (syst.) MeV, also yielded a similar χ^2 value.

1. Introduction. The introduction of the strangeness quantum number (S) adds a novel degree of freedom to conventional nuclear physics, opening the door to a new paradigm of hadron many-body systems [1,2]. Specifically, the involvement of strangeness degrees of freedom is expected to have significant importance in high-density hadronic matter reaching densities several times that of normal nuclear matter. Under such extreme density conditions, hyperons are predicted to emerge through the conversion of the large nucleon Fermi energy into hyperon mass. Neutron stars stand as a potential cosmic environment where these high-density conditions could manifest explicitly.

Hypernuclear spectroscopy has brought us important information on the hyperon (Y)– nucleon (N) and Y–Y interactions. For instance, the mass-number (A) dependence of energy levels within Λ single-particle orbits provides insights into the Λ potential depth $U_\Lambda(r)$ in nuclear matter, estimated to be approximately -30 MeV. Additionally, the fine structure of p-shell Λ hypernuclei has revealed spin-dependent interactions of the ΛN system.

In contrast to the relatively well-studied $S = -1$ hypernuclei (such as single Λ hypernuclei) [1], our current knowledge in $S = -2$ hypernuclei (such as Ξ and double Λ hypernuclei) remains limited. Several nuclear emulsion experiments reported results supporting the existence of bound Ξ-hypernuclear states. The High Energy Accelerator Research Organization (KEK) E373 experiment observed the KISO event [3,4], which is unambiguously ascribed to a Ξ-nucleus bound state. The unique decay mode of this event was identified as $\Xi^- + {}^{14}\mathrm{N} \to {}^{10}_{\Lambda}\mathrm{Be} + {}^{5}_{\Lambda}\mathrm{He}$. The binding energy of the Ξ^- hyperon, B_{Ξ^-}, in the ^{14}N nucleus was estimated to be $B_{\Xi^-} = 3.87 \pm 0.21$ or 1.03 ± 0.18 MeV, depending on whether the daughter $^{10}_{\Lambda}$Be hypernucleus is produced in the ground or excited state, respectively. In either case, the obtained binding energy significantly exceeds the 0.17 MeV binding energy of the $3D$ atomic states, where Ξ^- absorption is expected to take place.

Recently, in the J-PARC E07 experiment, twin hypernuclear events of the same type, IBUKI and IRRAWADDY, were further observed in nuclear emulsions. The IBUKI event [5] was uniquely identified to exhibit the same decay mode as the previously mentioned KISO event. The binding energy of IBUKI was determined to be $B_{\Xi^-} = 1.27 \pm 0.21$ MeV, suggesting a Coulomb-assisted nuclear $1p$ state. The decay mode of the IRRAWADDY event was uniquely assigned as $\Xi^- + {}^{14}\mathrm{N} \to {}^{5}_{\Lambda}\mathrm{He} + {}^{5}_{\Lambda}\mathrm{He} + {}^{4}\mathrm{He} + n$ [6]. The binding energy of IRRAWADDY was uniquely determined to be $B_{\Xi^-} = 6.27 \pm 0.27$ MeV because there is no excited state for the daughter particles.

Moreover, in the KEK E373 nuclear emulsion another $\Xi^- - {}^{14}\mathrm{N}$ system, known as the KINKA event, was observed [6]. The KINKA event exhibits a different decay mode: $\Xi^- + {}^{14}\mathrm{N} \to {}^{9}_{\Lambda}\mathrm{Be} + {}^{5}_{\Lambda}\mathrm{He} + n$. The evaluated binding energy was found to be relatively large, $B_{\Xi^-} = 8.00 \pm 0.77$ MeV for the ground state or 4.96 ± 0.77 MeV for the excited state of the daughter $^{9}_{\Lambda}$Be hypernucleus. The IRRAWADDY and KINKA events may correspond to the $1s$ state of the $^{15}_{\Xi}$C hypernucleus.

Based on these results obtained from the emulsion experiments, the interaction between Ξ and a nucleus is considered as attractive. Theoretical study following the nuclear emulsion data was reported in Ref. [7,8]. Nevertheless, it is important to note that the spectroscopic investigations are essential for assessing the binding energies of the Ξ hypernuclear states. The limited number of observed events in the nuclear emulsion experiments is insufficient because of a possible strong decay width originating from the $\Xi N - \Lambda\Lambda$ coupling in the Ξ hypernucleus.

Two experiments, KEK E224 [9] and BNL E885 [10], were performed to investigate the existence of Ξ hypernuclear bound states by measuring the missing-mass spectrum of the $^{12}\mathrm{C}(K^-, K^+)X$ reaction. The former measurement suggested a Ξ potential depth of approximately $V_0^\Xi \sim -20$ MeV. On the other hand, the latter provided better statistics and claimed evidence for the existence of the ${}^{12}_{\Xi}\mathrm{Be}$ bound state based on a spectrum shape analysis near the binding threshold. In the analysis, the potential depth of Ξ was estimated to be approximately $V_0^\Xi \sim -14$ MeV, assuming a Woods–Saxon-type potential. This potential depth resulted in a binding energy of the ${}^{12}_{\Xi}\mathrm{Be}$ ground state of approximately 4.5 MeV. However, due to the limited energy resolution of 14 MeV (full width at half maximum [FWHM]), it was not possible to observe any distinct peak corresponding to a bound state.

Moreover, a theoretical study comparing the experimental data and calculated spectra was reported by Kohno and Hashimoto [11]. In this theoretical study, the imaginary part associated with the absorption process $\Xi N \to \Lambda\Lambda$ was explicitly included. The effects of the absorption process were incorporated by convoluting the calculated spectrum with a Lorentz-type distribution function with an assumption of the full width $\Gamma = 4$ MeV. Here, the Ξ^- decay width in nuclear matter was investigated to be $\Gamma \sim 3$ MeV based on the measured total cross section of $4.3^{+6.3}_{-2.7}$ mb for the $\Xi^- p \to \Lambda\Lambda$ reaction [12] with the theoretical formula of Ref. [13]. These width values are almost consistent. The comparison showed that the potential with $V_0^\Xi \sim -14$ MeV did not agree with the Brookhaven National Laboratory (BNL) E885 data, and an almost zero potential was deemed preferable.

More recently, Harada and Hirabayashi investigated Ξ–nucleus potential using the old data of the BNL-E906 experiment [14], which measured the $^9\mathrm{Be}(K^-, K^+)$ reaction at 1.8 GeV/c [15]. In this study, both the real and imaginary parts of the Ξ–nucleus potential were varied for comparison. It has been found that an attractive potential with $V_0^\Xi = -17 \pm 6$ MeV, accompanied by a reasonable absorption of $W_0^\Xi = -5$ MeV for $\Xi^- p \to \Xi^0 n$ and $\Xi^- p \to \Lambda\Lambda$ transitions in the nuclear medium, provided the most suitable description of the data.

An alternative experimental method to investigate the Ξ–nucleus interaction is through Ξ^- atomic X-ray spectroscopy. The X-ray energy will be shifted and/or broadened due to the Ξ–nucleus strong interaction and the measurements of the energy shift and width give us information on the Ξ–nucleus potential. In this regard, the J-PARC E07 experiment pioneered measurement of coincident X-rays [16]. They tried to measure the X-ray emitted from Ξ^-–Br and Ξ^-–Ag atoms using germanium detectors by stopping Ξ^- in the nuclear emulsion. Furthermore, the J-PARC E03 experiment focused on the detection of X-rays from Ξ^-–Fe atoms. In this experiment, Ξ^- particles were produced via the (K^-, K^+) reaction in a thick iron target and stopped in it. X-rays were measured by germanium detectors. The analysis of the E03 experiment is currently in progress.

In a related research field, the interaction between two hadrons has been extensively studied through the measurement of the momentum correlation function, known as femtoscopy, in collaborations such as ALICE [17] and STAR [18]. In p−Pb collisions at $\sqrt{s_{NN}} = 5.02$ TeV at

the Large Hadron Collider, the ALICE collaboration observed attractive interaction between a proton and a Ξ^- through their correlation function [19]. Moreover, the measured correlation function exhibited consistency with recent lattice calculations conducted by the HAL QCD Collaboration [20]. The HAL QCD Collaboration employed $(2+1)$-flavor lattice quantum chromodynamics (QCD) simulations near the physical point and focused on studying the S-wave interactions of $\Lambda\Lambda$ and ΞN systems. It was found that the isospin-singlet and spin-singlet channel ($^{11}S_0$), which is coupled to the H-dibaryon, has the most attractive behavior in the ΞN system. In contrast, the ΞN ($^{31}S_0$) interaction was found to be weakly repulsive, whereas the ΞN ($^{13}S_1$) and ΞN ($^{33}S_1$) interactions exhibited weak attraction. Additionally, the HAL QCD Collaboration highlighted a weak coupling strength between $\Lambda\Lambda$ and ΞN at low energies. Furthermore, a detailed comparison was made between the momentum correlation functions of $S=-2$ baryon pairs ($p\Xi^-$ and $\Lambda\Lambda$) measured by the ALICE Collaboration [19] and the recent HAL QCD potential, taking into account the coupled channel effect [21]. The good agreement between the theory based on the HAL QCD potential and the experiment indicates that the ΞN interaction is moderately attractive without having a quasibound state.

2. J-PARC E05 experiment. In 2015, we carried out the J-PARC E05 experiment to investigate the existence of ${}^{12}_{\Xi}$Be bound states using the ${}^{12}\mathrm{C}(K^-, K^+)X$ reaction. The experimental data were collected at the K1.8 beamline of the Hadron Experimental Facility in J-PARC. A typical K^- beam intensity was about 6×10^5 particles per accelerator cycle of 5.52 seconds with a typical K/π ratio of ~ 0.8 and a beam spill length of ~ 2 seconds. For this experiment, a 9.364 g/cm^2 graphite target with natural isotope abundance was employed. A total number of 84.9×10^9 K^- particles with a momentum of 1.8 GeV/c impinged on it. Additionally, calibration data were collected using a 9.538 g/cm^2-thick polyethylene $[(C_2H_4)_n]$ target.

Figure 1 shows the schematic view of the experimental setup; the detail is described in Ref. [22]. The incident K^- beam was analyzed using the K1.8 beamline spectrometer [23]. The momenta of beam particles were reconstructed using the spatial information provided by scintillating fiber trackers and drift chambers, positioned upstream and downstream of quadrupole (Q) and dipole (D) magnets ($Q10$, $Q11$, $D4$, $Q12$, and $Q13$), respectively. For the momentum reconstruction, a third-order transfer matrix was employed. The design value of the momentum resolution was $\Delta p/p = 3.3\times10^{-4}$ (FWHM). The beam K^- was selected requiring the anticoincidence of the aerogel Čerenkov counters (BAC1 and BAC2) as $\overline{BAC1}\times\overline{BAC2}$ at the trigger level. The refractive index of the BACs is $n=1.03$, where the π detection efficiency at 1.8 GeV/c of BAC1 and BAC2 is 99.1% and 99.5%, respectively. Moreover, we identified K^- particles using the time-of-flight information of two sets of scintillator hodoscopes, BH1 and BH2, positioned upstream and downstream of the $QQDQQ$ magnets, respectively.

The outgoing particles, namely K^+ and proton, were detected and measured by the Superconducting Kaon Spectrometer (SKS) [23] configured in the "SksMinus setup" [24]. To analyze the outgoing K^+ particles originating from the Ξ-hypernucleus production, the SKS magnetic field was set to 2.49 T. These K^+ particles had a momentum of $\sim$1.4 GeV/c and were detected within a scattering angle range of $0^\circ < \theta_{K^+} \lesssim 20^\circ$. The SKS has a large acceptance in both angular coverage ($\sim$ 120 msr) and momentum range (1.1–2.4 GeV/c). The momentum reconstruction was performed by using hit information from the drift chambers positioned upstream and downstream of the SKS dipole magnet, along with a calculated magnetic field map based on the Runge–Kutta method. The achieved momentum resolution at 1.35 GeV/c was $\Delta p/p = 3.6\times10^{-3}$ (FWHM).

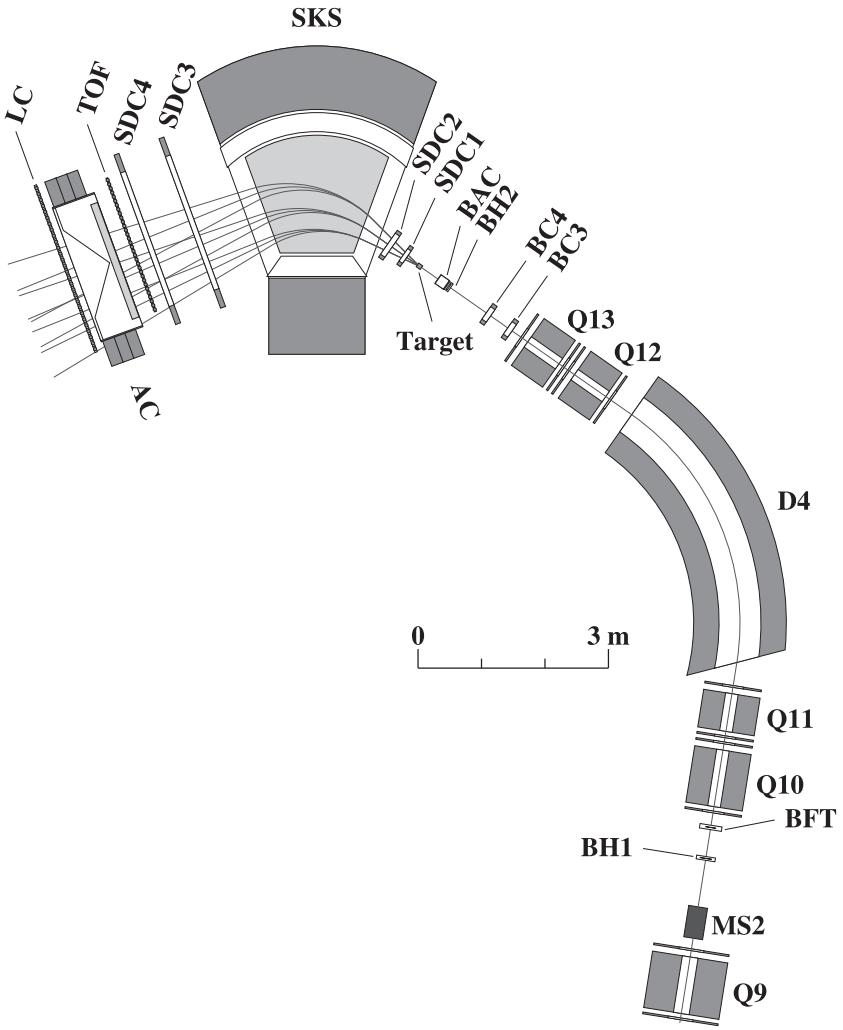

Fig. 1. Schematic view of the experimental setup taken from Ref. [22]. BCs and SDCs are drift chamber installed in the K1.8 beamline spectrometer and SKS, respectively. BFT is plastic scintillating fiber detector. MS is mass slit placed upstream of the K1.8 beamline spectrometer.

The outgoing K^+ was roughly selected by requiring anticoincidence of an aerogel Čerenkov counter (AC) with a refractive index $n = 1.05$, and coincidence of a Lucite Čerenkov counter (LC) with refractive index $n = 1.49$, at the trigger level. In the offline analysis, identification of the outgoing particles was performed by selecting a proper region of squared mass,

$$M^2_{\rm scat} = \left(\frac{p}{\beta}\right)^2 (1-\beta^2), \tag{1}$$

where p is the reconstructed momentum, and β is the velocity of the outgoing particle. β was calculated using the information of the flight path length and time-of-flight provided by the scintillator hodoscopes, BH2 and TOF, positioned upstream and downstream of the SKS magnet, respectively. The detail of the J-PARC E05 experiment is described in Ref. [22].

3. Analysis. The missing mass, M_X, for the $^{12}{\rm C}(K^-, K^+)X$ reaction can be evaluated as

$$M_X = M_{(K^-,K^+)} = \sqrt{(E_{K^-} + M(^A Z) - E_{K^+})^2 - (p^2_{K^-} + p^2_{K^+} - 2p_{K^-}p_{K^+}\cos\theta_{K^-K^+})}. \tag{2}$$

In this equation, E_{K^-} and p_{K^-} represent the energy and momentum of the incident K^- beam in the laboratory frame, while E_{K^+} and p_{K^+} correspond to the energy and momentum of the outgo-

ing K^+ particle, respectively. The symbols A and Z denote the mass number and nuclear charge, respectively. Namely, $A = 12$ and $Z = 6$ for the ^{12}C nucleus. $M(^AZ)$ represents the mass of the target nucleus, namely ^{12}C mass. The $\theta_{K^-K^+}$ represents the scattering angle of the (K^-, K^+) reaction. Therefore, in order to calculate the missing mass, three kinematic variables need to be measured: p_{K^-}, p_{K^+}, and $\theta_{K^-K^+}$. These variables are obtained through momentum reconstruction after the event selection. Once the missing mass is determined, the binding energy of Ξ^-, B_{Ξ^-}, can be calculated as:

$$B_{\Xi^-} = M(^{(A-1)}(Z-1)) + M_{\Xi^-} - M_X, \tag{3}$$

where $M(^{(A-1)}(Z-1))$ is the mass of the core nucleus, namely ^{11}B mass. M_{Ξ^-} is the mass of the Ξ^- particle. In this calculation, we used the values of $M(^{11}\mathrm{B}) = 10252.55$ MeV/c^2 and $M_{\Xi^-} = 1321.71$ MeV/c^2.

The double differential cross section, $(d^2\bar{\sigma}/d\Omega/dM)_{\theta_1\text{-}\theta_2}$, for the $^{12}\mathrm{C}(K^-, K^+)X$ reaction averaged over the scattering angle from θ_1 to θ_2, can be evaluated as a function of the missing mass by the equation:

$$\left(\frac{d^2\bar{\sigma}}{d\Omega dM}\right)_{\theta_1\text{-}\theta_2} = \frac{1}{N_{\mathrm{target}}}\frac{N_{K^-K^+}}{N_{\mathrm{beam}}\Delta\Omega_{\theta_1\text{-}\theta_2}\Delta M\epsilon}. \tag{4}$$

In this equation, N_{target} represents the number of target nuclei inside the target material, $N_{\mathrm{target}} = 4.7 \times 10^{23}$ for the graphite target. $N_{K^-K^+}$ represents the number of valid (K^-, K^+) events within the missing-mass interval ΔM. N_{beam} represents the number of incident beam kaons on the target, $N_{\mathrm{beam}} = 5.2 \times 10^{10}$ for the graphite target data. $\Delta\Omega_{\theta_1\text{-}\theta_2}$ represents the effective solid angle of the SKS between θ_1 and θ_2, where the SKS has an acceptance of about 120 msr. ϵ represents the total experimental efficiency including the K^+ decay factor, with a typical value of $\epsilon \sim 24\%$.

The analysis for the (K^-, K^+) reaction searching for the Ξ-hypernucleus and the analysis for the (K^-, p) reaction studying the $\bar{K}$–nucleus interaction, which was reported in Ref. [22], share commonalities in terms of analysis techniques and methodologies. This includes the momentum correction procedure. In fact, the analysis of the $p(K^-, K^+)\Xi^-$ reaction was also used for the momentum correction in Ref. [22] for accurate determination of the absolute momenta and estimation of the systematic uncertainties.

4. Experimental results. First, we present the proton-target data analysis at $p_{K^-} = 1.8$ GeV/c. Figure 2(a) displays the double differential cross section extracted from the CH_2 target data as a function of the missing mass, $M_{(K^-,K^+)}$. The spectrum was obtained assuming the reaction target to be a proton. In this plot, a scattering angle selection of $4^\circ < \theta_{\mathrm{Lab}} < 6^\circ$ was applied. The spectrum was fitted using a combination of a Gaussian function and a third-order polynomial as drawn by a red curve. The green dashed curve represents the Gaussian component corresponding to the elementary Ξ^- production. The third-order polynomial component is attributed to quasi-free (QF) Ξ production, specifically the K^-"p" $\to K^+\Xi^-$ reaction, where "p" denotes the proton within the carbon nucleus of the polyethylene CH_2 material. The spectrum is expected to broaden due to nucleon Fermi-motion within the carbon nucleus.

To estimate the differential cross section of the $p(K^-, K^+)\Xi^-$ reaction, we integrated the Gaussian component as shown in Fig. 2(b). In this plot, we compare the evaluated differential cross section with the past data reported in Ref. [25]. Note that the evaluated differential cross section exhibits reasonable agreement with the old data, even though the statistical pre-

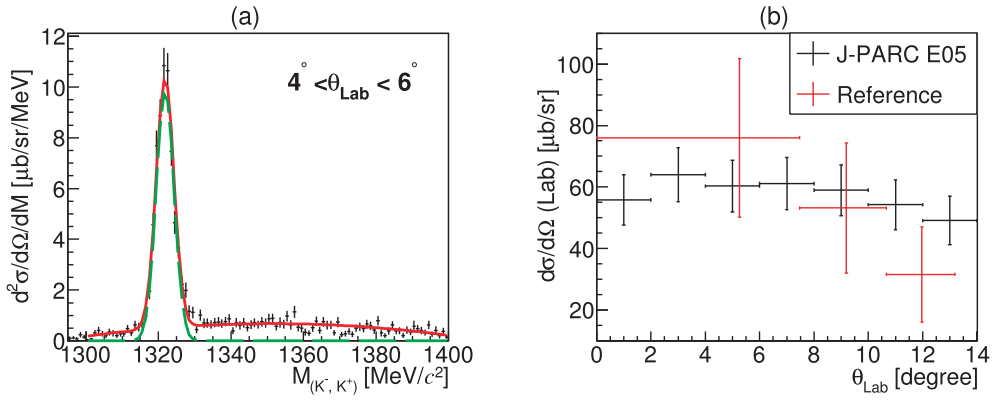

Fig. 2. (a) Missing-mass spectrum of the $p(K^-, K^+)$ reaction extracted from the CH_2 target data in the $4^\circ < \theta_{\rm Lab} < 6^\circ$ interval. The vertical axis is given as a double differential cross section. The spectrum is fitted by using a combination (red line) of a Gaussian function and a third-order polynomial. The Gaussian component, corresponding to the elementary Ξ^- production, is depicted by the green dashed line. (b) Comparison of the differential cross section for the $p(K^-, K^+)\Xi^-$ reaction at $p_{K^-} = 1.8$ GeV/c. The present result is represented by black points with statistical errors. Data from Ref. [25] are displayed as red points for comparison.

cision of Ref. [25] is significantly worse. A detailed comparison of these data with theoretical calculations, such as those referenced in Ref. [26], will clarify the reaction mechanism.

The missing-mass resolution could be understood through the analysis of the CH_2 spectrum. It can be decomposed into contributions from the momentum ($\Delta_{\rm mom}$) and angular (Δ_θ) resolutions, and the energy-loss straggling ($\Delta_{\rm E}$). Assuming the momentum resolution of the beamline spectrometer to be $\Delta p/p = 3.3 \times 10^{-4}$ (design value) in FWHM, the momentum resolution of the SKS was evaluated to be $\Delta p/p = 3.6 \times 10^{-3}$ (FWHM) at 1.35 MeV/c by the beam pass-through data analysis. The angular resolution was also estimated to be 14 mrad (FWHM) by the beam pass-through data analysis. The energy-loss straggling term Δ_E was estimated by a Monte-Carlo simulation. The subcontributions in the $p(K^-, K^+)\Xi^-$ kinematics were estimated to be $\Delta_{\rm mom} = 4.2$ MeV/c^2, $\Delta_\theta = 2.6$ MeV/c^2, and $\Delta_{\rm E} = 1.8$ MeV/c^2. The overall missing-mass resolution in the $p(K^-, K^+)\Xi^-$ kinematics was estimated to be 5.8 MeV (FWHM) by the Monte-Carlo simulation, based on these subcomponents. The simulated mass resolution was consistent with the obtained missing-mass resolution in the $p(K^-, K^+)\Xi^-$ spectrum shown in Fig. 2(a). It should be noted that the overall resolution is not a simple square-root sum of each subcomponent because the energy-loss straggling ($\Delta_{\rm E}$) has a non-Gaussian form. In the $^{12}C(K^-, K^+)$ kinematics, the subcontributions were $\Delta_{\rm mom} = 6.3$ MeV, $\Delta_\theta = 1.3$ MeV, and $\Delta_{\rm E} = 4.2$ MeV. The overall energy resolution in the $^{12}C(K^-, K^+)$ reaction around the threshold energy ($B_{\Xi^-} \sim 0$) was estimated to be 8.2 MeV (FWHM).

The absolute momentum scales measured by the K1.8 beamline and SKS spectrometers were adjusted using a combination of $p(K^-, K^+)\Xi^-$, $p(K^-, p)K^-$, and beam pass-through data analyses [22]. The momenta were corrected with polynomial functions to reduce the difference between the Particle Data Group values and the measured values of the K^- and Ξ^- masses, as well as to address the momentum difference (dp) between the two spectrometers using the beam pass-through data. The momentum difference, dp, was obtained by comparing the measured momenta from the K1.8 beamline and SKS spectrometers as $dp = p_{\rm SKS} - p_{\rm K1.8}$. The systematic uncertainty in determining the binding energy for the $^{12}C(K^-, K^+)$ reaction around

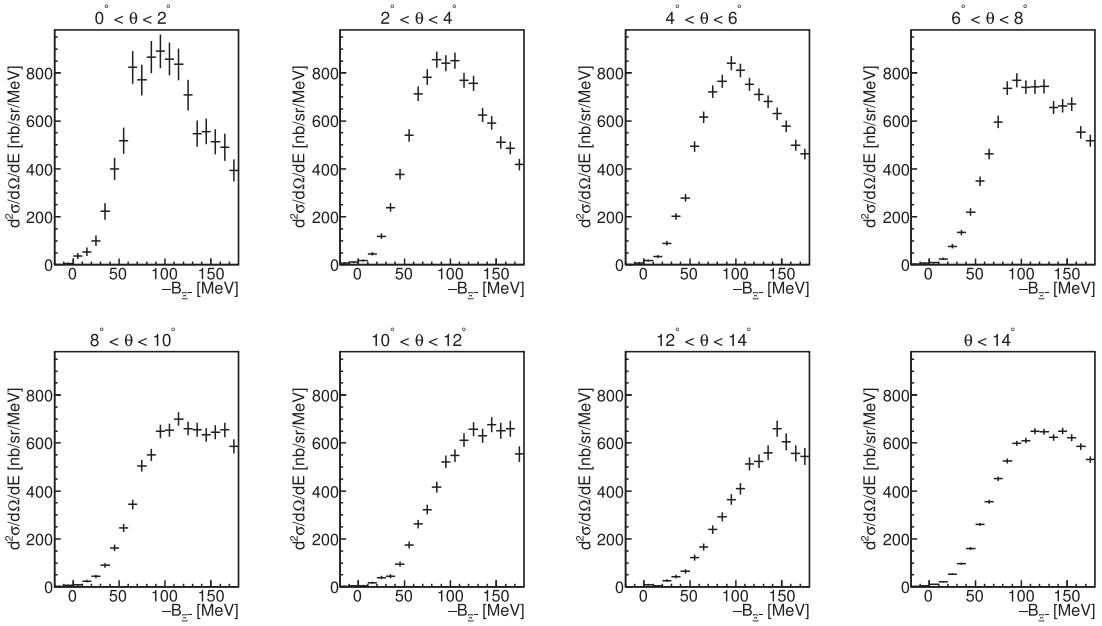

Fig. 3. Double differential cross section of the ^{12}C target data as a function of the Ξ-binding energy, B_{Ξ^-}. The title of each plot shows the scattering angle range selected in the laboratory system.

the threshold energy ($B_{\Xi^-} \sim 0$) was estimated to be ±0.5 MeV by considering the difference between the ideal and corrected momenta after the absolute momentum adjustment.

Next, we present results of the graphite-target data analysis at $p_{K^-} = 1.8$ GeV/c. Figure 3 shows the double differential cross section of the ^{12}C(K^-, K^+) reaction as a function of the Ξ-binding energy, B_{Ξ^-}. Our measurements cover a wide energy range with precise scattering angle selection at 2-degree intervals in the laboratory frame. Note that high-precision and high-statistics (K^-, K^+) reaction data are presented for the first time. By performing a comprehensive comparison between these spectra and theoretical calculations, the Ξ–nucleus potential will be investigated in the future, as done in previous studies [11,15].

Figure 4 shows the Ξ binding-energy spectrum around the Ξ binding threshold region, $B_{\Xi^-} \sim 0$. In Fig. 4(a), a 2D plot of B_{Ξ^-} vs. $M^2_{\rm scat}$ of the outgoing particles, as described in Eq. (1), is displayed. The outgoing K^+ particles were selected using a gate defined as $0.175 < M^2_{\rm scat} < 0.300$ (GeV/c^2)^2, which corresponds to ±2 standard deviations, as indicated by the red dashed lines. As seen in this figure, the K^+ structure is clearly distinguishable in the $M^2_{\rm scat}$ distribution, even in the bound region where $B_{\Xi^-} > 0$. However, we found that background components are present also within the K^+ selection gate.

To address this point, we carefully examined the squared mass ($M^2_{\rm scat}$) distribution for each binding energy region as shown in Fig. 5, where the selection region of B_{Ξ^-} is denoted in the title of each plot. Subsequently, a two-component fit was performed on the $M^2_{\rm scat}$ distribution. The total fit results are represented by the red curves, and the subcomponents corresponding to the outgoing K^+ particles and background are shown by the green and blue dashed curves, respectively. In this fit, Gaussian distributions were employed to model the outgoing K^+ component, with the fixed mean value and the standard deviation, which were determined by fitting the unsliced squared mass distribution.

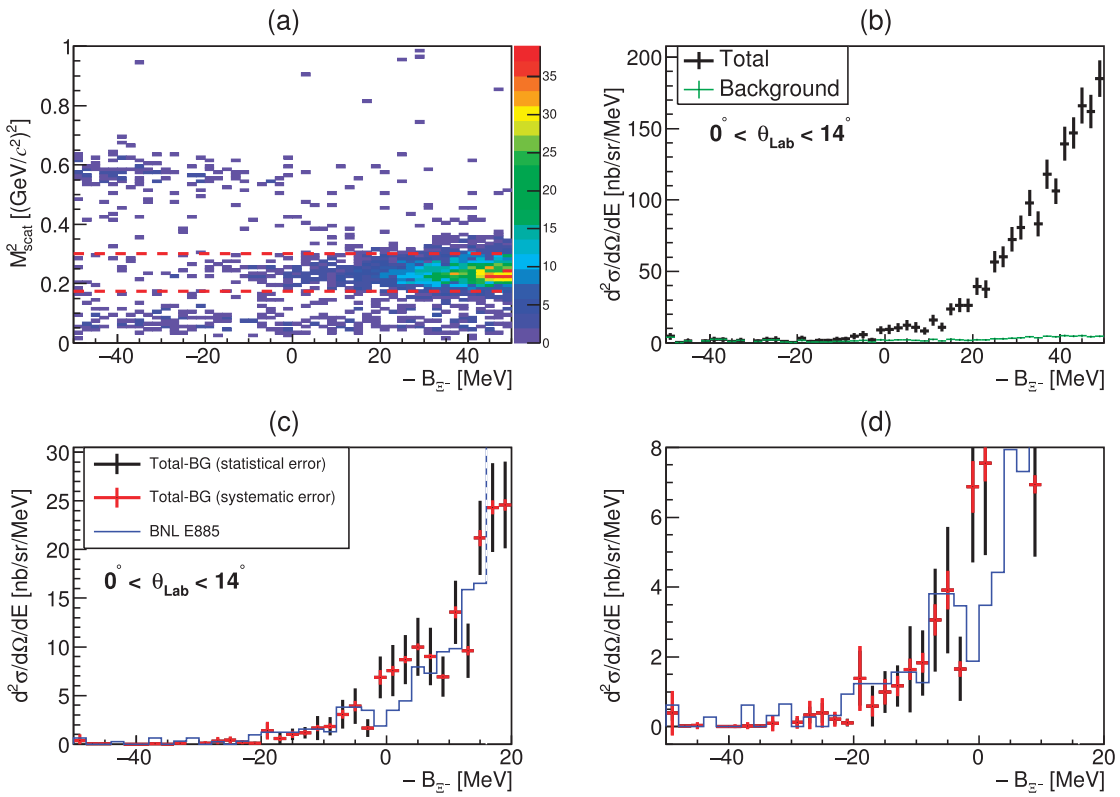

Fig. 4. (a) 2D plot of $M^2_{\rm scat}$ of the outgoing particles as a function of B_{Ξ^-} around the binding energy threshold. (b) Double differential cross section of ^{12}C(K^-, K^+) reaction around the threshold region. The background contamination due to the misidentification of the outgoing particles is shown by the green points with error bars. (c) Comparison between the present spectrum and the past BNL E885 experimental spectrum reported in Ref. [10]. BG, background. See detail in the text. (d) Enlarged view of panel (c) to see the small cross section region.

We assumed linear or exponential functions for the background distribution in the $M^2_{\rm scat}$ plots. In Fig. 5, the results with the linear background function are shown. By integrating the signal Gaussian (green curve) and the background functions (blue curve) within the $M^2_{\rm scat}$ selection gate ($0.175 < M^2_{\rm scat} < 0.300$ (GeV/c^2)^2), the fractions of the outgoing K^+ signal ($N_{\rm S}$) and background ($N_{\rm BG}$) were estimated. The background contribution in the B_{Ξ^-} spectrum was then evaluated, as shown by the green points with error bars in Fig. 4(b), by multiplying the fraction ratio $\frac{N_{\rm BG}}{N_{\rm S}+N_{\rm BG}}$. The error bars represent the systematic uncertainty originating from the ambiguity in the fraction ratio $\frac{N_{\rm BG}}{N_{\rm S}+N_{\rm BG}}$ estimation. This uncertainty was estimated by checking the stability of the fraction ratio $\frac{N_{\rm BG}}{N_{\rm S}+N_{\rm BG}}$ when changing the assumed background function (linear or exponential) and varying the selected region of the Ξ-binding energy.

The double differential cross section before background subtraction is shown by the black points with statistical error bars in Fig. 4(b). The spectrum after the background subtraction is displayed in Fig. 4(c) and an enlarged view to see the small cross section region is shown in Fig. 4(d). The statistical errors are represented by the black bars, whereas the systematic error stemming from the background estimation is denoted by the red bars. This final spectrum is then compared with the BNL E885 experiment results [10], shown as a blue histogram. As seen in this figure, we found that our spectrum is in reasonable agreement with the past BNL E885's spectrum. The consistency of the absolute cross section provides further support for the

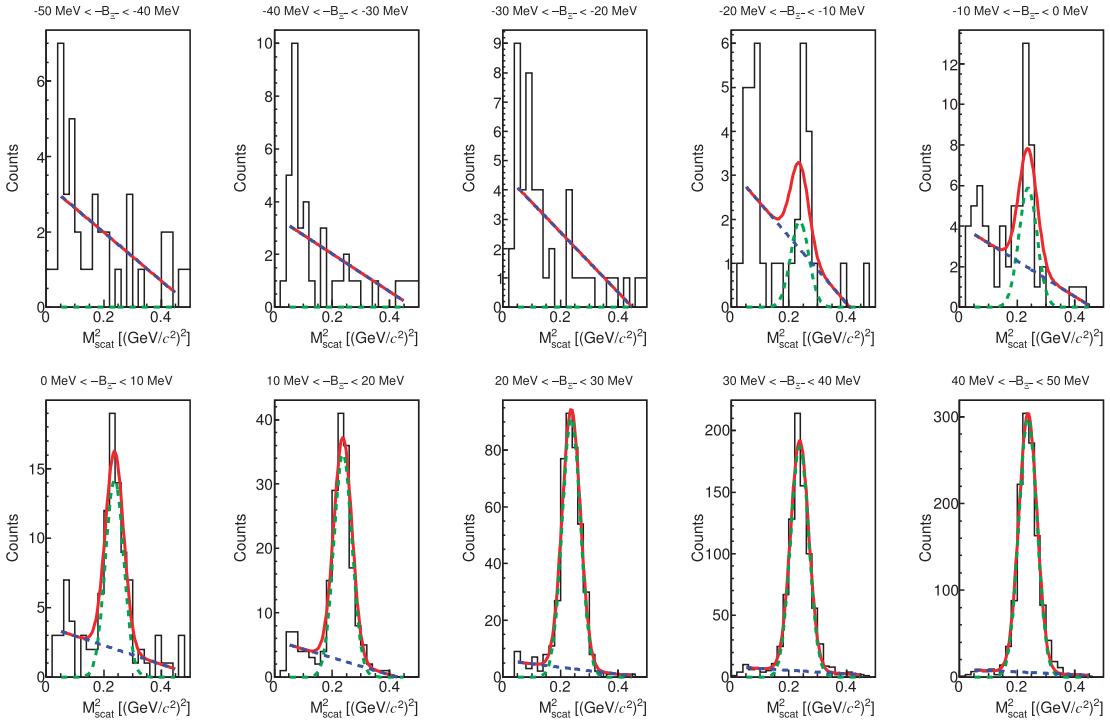

Fig. 5. Squared mass, $M^2_{\rm scat}$, distribution of the outgoing particles analyzed by the SKS for each Ξ-binding energy region. The title of each plot shows the selected region of Ξ-binding energy. See detail in the text.

Table 1. Summary of the spectrum-fitting results shown in Fig. 6.

Function	χ^2/ndf (ndf)	P-value	Fitting parameters (MeV)
(a) QF($\Gamma = 0$) + 1Gaus	1.83 (23)	0.00896	$B_{\Xi^-} = 7.1 \pm 1.5$ (stat.) $^{+2.4}_{-6.1}$ (syst.)
(b) QF($\Gamma = 0$) + 2Gaus	0.849 (22)	0.665	$B^{\rm 1st}_{\Xi^-} = 8.9 \pm 1.4$ (stat.) $^{+3.8}_{-3.1}$ (syst.)
			$B^{\rm 2nd}_{\Xi^-} = -2.4 \pm 1.3$ (stat.) $^{+2.8}_{-1.2}$ (syst.)
(c) QF($\Gamma \neq 0$) + 1BW	0.954 (23)	0.524	$B_{\Xi^-} = -2.7 \pm 2.2$ (stat.) $^{+0.5}_{-0.7}$ (syst.)
			$\Gamma = 4.1 \pm 2.1$ (stat.) $^{+1.2}_{-0.7}$ (syst.)
(d) QF($\Gamma = 0$)	2.49 (19)	0.000332	
(e) QF($\Gamma \neq 0$)	1.39 (25)	0.0914	$\Gamma = 8.7 \pm 1.1$ (stat.)

reliability and accuracy of the two datasets in the Ξ-binding energy spectrum near the threshold region.

5. Discussion. To understand the obtained B_{Ξ^-} spectrum, we performed spectrum fitting under several hypotheses, as shown in Fig. 6. The error bars in this figure represent the quadratic sum of statistical and systematic errors, shown by the black and red bars of Fig. 4(c), respectively. The fit results are summarized in Table 1.

In all the trials, we assumed that the dominant part of the unbound region, $B_{\Xi^-} < 0$, can be described by the QF Ξ production. We adopted a phenomenological fit function for the QF Ξ production given as

$$h(B'_{\Xi^-}) = C\sqrt{B'_{\Xi^-}}\exp(\alpha B'_{\Xi^-} + \beta B'^2_{\Xi^-}), \tag{5}$$

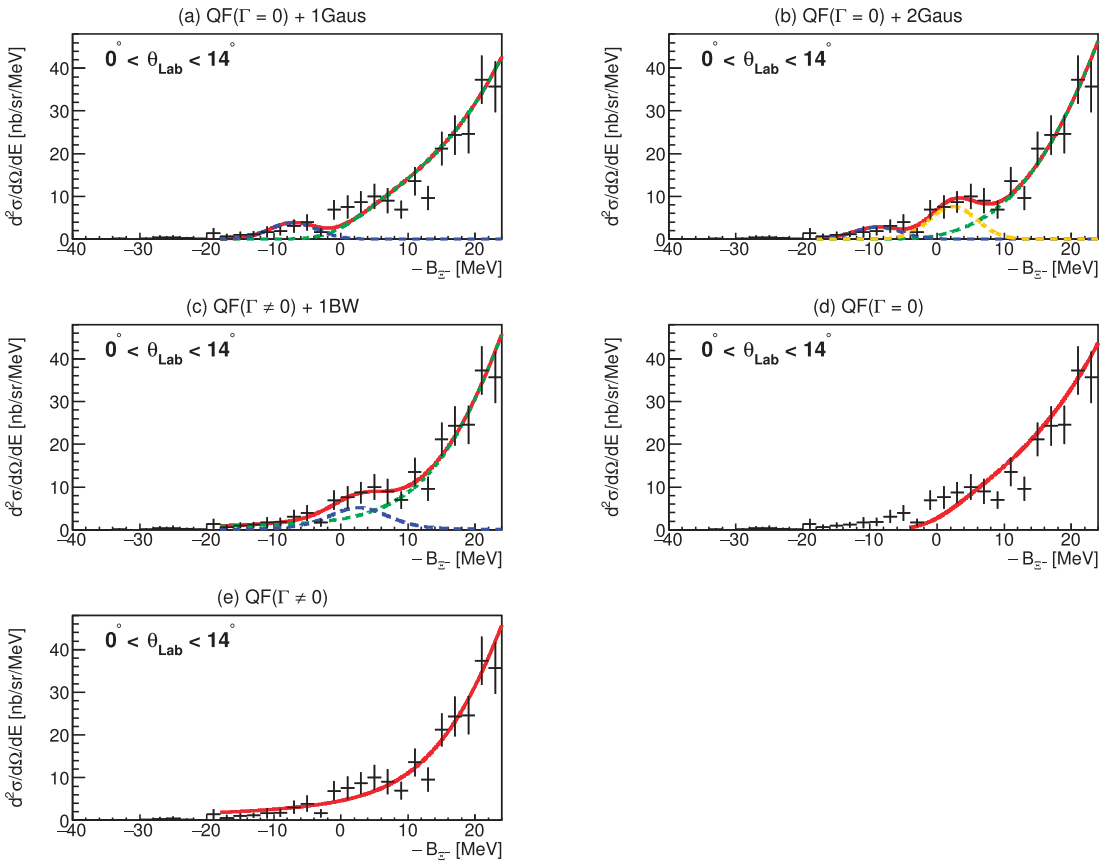

Fig. 6. B_{Ξ^-} spectrum fitting under different hypotheses. The assumed functions are shown in the title of each plot. The total fit result is shown by the red curves. The different contributions are shown by curves in different colors. See text for further details. BW, Breit–Wigner.

where $B'_{\Xi^-} = -B_{\Xi^-}$, α and β are the fitting parameters, and C represents a normalization factor. The QF spectrum should be smeared by the experimental energy resolution and $\Xi N \to \Lambda\Lambda$ conversion. These effects were included by convoluting Eq. (5) with a Voigt function [27], where the σ parameter was fixed to the experimental energy resolution ($\sigma = 3.5$ MeV).

Considering that the HAL QCD Collaboration predicts a weak coupling strength between $\Lambda\Lambda$ and ΞN [20], the $\Xi N \to \Lambda\Lambda$ conversion effect may be negligibly small compared to the experimental resolution. Therefore, in assumptions (a), (b), and (d) of Table 1, the Γ of the convoluting Voigt function was fixed to $\Gamma = 0$, meaning that in these cases the QF function (Eq. 5) was convoluted with a Gaussian function.

In assumptions (a), (b), and (c) of Table 1, we assumed the existence of the Ξ-hypernuclear state, whereas the null hypothesis is tested in assumptions (d) and (e). In assumption (a), we added a Gaussian component corresponding to the Ξ-hypernuclear state. In this case, we assumed that the $\Xi N \to \Lambda\Lambda$ conversion width is negligibly small compared to our experimental resolution. The added Gaussian and QF components are displayed by the blue and green dashed curves, respectively, in Fig. 6(a).

In assumption (b), we added two Gaussian components, assuming that an excited state also exists. Several prominent peak structures are theoretically expected due to the ^{11}B core's excited states [28], where the excitation energy depends on the strength of the spin-spin interaction. The

added two Gaussian components are shown by the blue and orange dashed curves in Fig. 6(b), whereas the QF component is shown by the green dashed curve.

In assumption (c), we added one Breit–Wigner component, assuming the existence of a sizeable $\Xi N \to \Lambda\Lambda$ conversion width. In this fitting, we added one Voigt function, where the parameter Γ was commonly varied with the convoluting Voigt function of the QF function. The parameter σ of the added Voigt fuction was also fixed to the value of the experimental resolution. The added Voigt and QF components are displayed by the blue and green dashed curves, respectively.

In contrast, in assumptions (d) and (e), no extra peak was assumed and the spectra were fitted without adding any Gaussian or Breit–Wigner component. These assumptions serve as null hypotheses, testing whether any additional peaks beyond the QF Ξ production are required to describe the data.

A summary of the χ^2/ndf, P-value, and the fitting parameters obtained for each assumption are listed in Table 1. The systematic errors of the binding energy and the width (Γ) were estimated by varying the fitting range, the spectrum binning, and the QF functions in the following way:

$$h'(B'_{\Xi^-}) = CB'_{\Xi^-}\exp(\alpha B'_{\Xi^-} + \beta B'^2_{\Xi^-}). \tag{6}$$

As seen in Table 1, both of assumptions (b) and (c) give reasonable χ^2/ndf values, whereas the other assumptions including the null hypothesis are rejected. Thus, this result indicates the existence of some structure around the Ξ binding threshold. The nuclear emulsion experiments also reported the Ξ-hypernuclear states, as described in Section 1, supporting our indications of the existence of the bound state. However, due to the limited statistics of the emulsion data and the limited sensitivity of our results, it is difficult to conclude the binding energy of the Ξ-hypernuclear states.

To determine the binding energy of Ξ-hypernuclear states and conclude which of assumptions (b) and (c) are correct, we need more sensitivity by improving the energy resolution. A future experiment, J-PARC E70 [29], is planned at J-PARC for this purpose. In this experiment, we aim to measure the $^{12}\mathrm{C}(K^-, K^+)$ spectrum with 2 MeV (FWHM) resolution using the S-2S spectrometer and Active Fiber Target (AFT) system. The 2 MeV resolution will make it possible to observe a clear and distinct peak structure if there is no large decay width. The J-PARC E70 experiment will play a crucial role in revealing the structure of the Ξ-hypernuclear states.

6. Conclusions. We have measured an inclusive spectrum in the $^{12}\mathrm{C}(K^-, K^+)$ reaction, using the SKS at the Hadron Experimental Facility in J-PARC. With high statistics and a good energy resolution of 8.2 MeV (FWHM), we explored a broad energy range with precise scattering angle selection. The resulting dataset offers a unique opportunity to compare theoretical calculations to determine the Ξ–nucleus potential.

Our results revealed that the absolute value of the measured cross section agrees well with the previous work of BNL E885 [10]. We employed a detailed spectrum-fitting procedure to test several assumptions near the threshold region. Our analysis showed that a good agreement with the spectrum was achieved by combining a QF background and two Gaussian functions with peak positions at $B_{\Xi^-} = 8.9 \pm 1.4\,(\mathrm{stat.})\,^{+3.8}_{-3.1}\,(\mathrm{syst.})$ MeV and $B_{\Xi^-} = -2.4 \pm 1.3\,(\mathrm{stat.})\,^{+2.8}_{-1.2}$ (syst.) MeV. An alternative assumption, including the QF and one Breit–Wigner function with $B_{\Xi^-} = -2.7 \pm 2.2\,(\mathrm{stat.})\,^{+0.5}_{-0.7}\,(\mathrm{syst.})$ MeV and $\Gamma = 4.1 \pm 2.1\,(\mathrm{stat.})\,^{+1.2}_{-0.7}\,(\mathrm{syst.})$ MeV, also gave

a similar χ^2 value. On the other hand, the null hypothesis was clearly rejected, indicating the presence of additional dynamics beyond the QF Ξ production contribution.

In conclusion, our experimental results provide valuable insights into the Ξ–nucleus potential and indicate the presence of additional dynamics beyond the QF Ξ production contribution. We are confident that the upcoming experiment will enable us to obtain more precise measurements and further advance our understanding of ΞN interaction.

Funding

The work was supported by Japan Society for the Promotion of Science (JSPS) KAKENHI Grant Numbers JP18H05403 and 17070006.

Acknowledgements

We would like to thank the staff of the J-PARC accelerator and the Hadron Experimental Facility for their great efforts on stable machine operation and beam quality improvements. We also acknowledge the efforts of the staff at KEK Computing Research Center for their support of our data analysis. The authors also thank SINET4.

References

[1] O. Hashimoto and H. Tamura, Prog. Part. Nucl. Phys. **57**, 564 (2006).
[2] A. Feliciello and T. Nagae, Rept. Prog. Phys. **78**, 096301 (2015).
[3] K. Nakazawa et al., Prog. Theor. Exp. Phys. **2015**, 033D02 (2015).
[4] E. Hiyama and K. Nakazawa, Ann. Rev. Nucl. Part. Sci. **68**, 131 (2018).
[5] S. H. Hayakawa et al., Phys. Rev. Lett. **126**, 062501 (2021).
[6] M. Yoshimoto et al., Prog. Theor. Exp. Phys. **2021**, 073D02 (2021).
[7] E. Friedman and A. Gal, Phys. Lett. B **820**, 136555 (2021).
[8] E. Friedman and A. Gal, Phys. Lett. B **837**, 137640 (2023).
[9] T. Fukuda et al. [E224 Collaboration], Phys. Rev. C **58**, 1306 (1998).
[10] P. Khaustov et al. [The AGS E885 Collaboration], Phys. Rev. C **61**, 054603 (2000).
[11] M. Kohno and S. Hashimoto, Prog. Theor. **123**, 157 (2010).
[12] J. K. Ahn et al., Phys. Lett. B **633**, 214 (2006).
[13] C. B. Dover, A. Gal, and D. J. Millener, Nucl. Phys. A **572**, 85 (1994).
[14] T. Tamagawa et al., Nucl. Phys. A **691**, 234c (2001).
[15] T. Harada and Y. Hirabayashi, Phys. Rev. C **103**, 024605 (2021).
[16] M. Fujita et al., Prog. Theor. Exp. Phys. **2022**, 123D01 (2022).
[17] S. Acharya et al. [ALICE Collaboration], Phys. Lett. B **797**, 134822 (2019).
[18] L. Adamczyk et al. [STAR Collaboration], Phys. Rev. Lett. **114**, 022301 (2015).
[19] S. Acharya et al. [ALICE Collaboration], Phys. Rev. Lett. **123**, 112002 (2019).
[20] K. Sasaki et al. [HAL QCD Collaboration], Nucl. Phys. A **998**, 121737 (2020).
[21] Y. Kamiya, K. Sasaki, T. Fukui, T. Hyodo, K. Morita, K. Ogata, A. Ohnishi, and T. Hatsuda, Phys. Rev. C **105**, 014915 (2022).
[22] Y. Ichikawa et al., Prog. Theor. Exp. Phys. **2020**, 123D01 (2020).
[23] T. Takahashi et al., Prog. Theor. Exp. Phys. **2012**, 02B010 (2012).
[24] T. O. Yamamoto et al. [J-PARC E13 Collaboration], Phys. Rev. Lett. **115**, 222501 (2015).
[25] D. A. Sharov, V. L. Korotkikh, and D. E. Lanskoy, Eur. Phys. J. A **47**, 109 (2011).
[26] S.-H. Kim, J. K. Ahn, S. H. Kim, S. Nam, and M.-K. Cheoun, Phys. Rev. C. **107**, 065202 (2023).
[27] J. Humlíček, J. Quant. Spectrosc. Rad. Trans. **21**, 437 (1982).
[28] T. Motoba and S. Sugimoto, Nucl. Phys. A **835**, 223 (2010).
[29] T. Nagae et al., (2018), J-PARC E70 proposal(http://j-parc.jp/researcher/Hadron/en/pac_1801/pdf/P70_2018-10.pdf).